JOURNAL OF COMPUTATIONAL PHYSICS 112, 31–43 (1994)

Multicomponent Flow Calculations by a Consistent Primitive Algorithm

SMADAR KARNI*

Department of Mathematics, University of Michigan, Ann Arbor, Michigan 48109

Received November 4, 1991; revised March 25, 1993

The dynamics of inviscid multicomponent fluids may be modelled by the Euler equations, augmented by one (or more) additional species equation(s). Attempts to compute solutions for extended Euler models in conservation form, show strong oscillations and other computational inaccuracies near material interfaces. These are due to erroneous pressure fluctuations generated by the conservative wave model. This problem does not occur in single component computations and arises only in the presence of several species. A nonconservative (primitive) Euler formulation is proposed, which results in complete elimination of the oscillations. The numerical algorithm uses small viscous perturbations to remove leading order conservation errors and is conservative to the order of numerical approximation. Numerical experiments show clean monotonic solution profiles, with acceptably small conservation error for shocks of weak to moderate strengths.

1. INTRODUCTION

The dynamics of compressible inviscid fluids may be modelled by the Euler equations. These are nonlinear hyperbolic partial differential equations (PDEs), describing the conservation of mass, momentum, and energy. If the fluid consists of several components, species equations are added which describe the conservation of the species.

A cornerstone in the computation of solutions to hyperbolic conservation laws is that the conservation form of the equations provides the best flow description. In practice, while this may be true for flows dominated by strong shocks, it may not be the case for flows dominated by other flow phenomena. For example, attempting to compute multicomponent fluid dynamics via extended Euler models in conservation form gives rise to oscillations and other computational inaccuracies near material interfaces [1, 11, 12]. These are *not* the common oscillations associated with high order numerical schemes. They are present already in *first*-order calculations and are hard to eliminate by going to higher order schemes. They are produced by the best available numerical schemes, including Godunov, Roe, Osher, and van Leer. If the interface happens to separate between reactive and nonreactive gas components, clearly such oscillations lead to incorrect energy balance. In such cases, one may be prepared to sacrifice strict conservation in favour of a better description of the dominant flow phenomena and to write the equations in nonconservative (primitive) form.

Indeed, the choice of the primitive set of variables that includes density, velocity, and pressure provides a model better suited for computations of propagating material fronts and results in clean and monotonic solution profiles. In fact, near material interfaces the governing equations reduce to *linear* advection of density (temperature) gradients and thus, although nonconservative, the model becomes *exact* and does not induce any conservation errors (see also [8]). Near shocks, however, conservation errors are committed and the primitive model is generally unsatisfactory. Computed solutions, although oscillation-free near material fronts, give physically inconsistent shocks which do not satisfy the shock jump conditions.

A viscous perturbation technique has been derived by the author [10], based on an idea in [22], which removes the leading order conservation errors and results in a "nearly" conservative model, which is conservative to the order of the numerical approximation in smooth parts of the solutions. Inside the numerical shock transition, the conservation errors, althoug greatly reduced, are still $O(1)$ and so they do not vanish under mesh refinement. This is in agreement with Hou and Le Floch [9], who show that nonconservative schemes converge to weak solutions of conservation laws with source terms that do not vanish near shocks.

Using a nonconservative flow description may not be the only way to eliminate the oscillations near propagating material fronts. Another possibility is to use extrapolation techniques similar to the ones proposed in [4], where conservation laws with stiff source terms are shown to produce

* Research supported in part by ONR Grant N00014-92-J-1245 and by NSF Grant DMS92 03768. Present address: Courant Institute, New York University, 251 Mercer Street, New York, NY 10012.

581/112/1-3

0021-9991/94 $6.00

wrong shock speeds. Extrapolation techniques are also used in shock reconstruction by subcell resolution [7]. The main difficulty with such techniques is identifying the direction of extrapolation. These techniques are fine for one-dimensional computations, but their extension to higher space dimensions is not trivial. Another strategy is to use a genuinely nonconservtive algorithm throughout the flow field and to revert to a conservative scheme near shocks. In [6, 9], it is shown that such hybrid scheme converge to correct weak solutions. However, switching strategies and extensions to higher dimensions are, again, not easy. Moreover, they may end up defeating the purpose of going nonconservative, namely the clean capturing of propagating material fronts.

The genuinely primitve algorithm used in this paper has been tested extensively in [10]. It was found to produce acceptably small conservation errors for shocks of weak to moderate strengths. It thus allows wave computation in multispecies flows which are both oscillation-free near material fronts and have only small conservation errors.

The outline of this paper is as follows. In Section 2, we describe various extensions of the single component Euler model to multicomponents, both in conservation and in primitive form. A brief description of the viscous perturbation numerical algorithm of [10] is also given. Section 3 contains simple wave analysis of the various models and points out several wave modelling differences between the conservative and the primitive formulations. In Section 4, the approximate Riemann solver for the extended Euler models is described, based on Roe's local linearization. Section 5 analyzes the various models with respect to their capability to model propagating material interfaces. Section 6 presents numerical evidence in support of the claim that the nonconservative flow description does a better job in modelling propagating material interfaces.

2. MODELS FOR MULTISPECIES FLOW PROBLEMS

The following discussion in specialized, although not limited, to two component flows in one space dimension. We use ρ, u, p, E, $H=(E+p)/\rho$ and a to denote density, velocity, pressure, total energy, total enthalpy per unit mass, and the speed of sound; i denotes the internal energy per unit mass; C_p and C_v are the specific heats at constant pressure/volume, respectively. In the case of ideal gases, $i=p/\rho(\gamma-1)$ and $a^2=\gamma p/\rho$, where γ is the ratio of specific heats and is constant for each species. In this notation, the single component Euler equations in conservation form are

$$\begin{pmatrix}\rho\\ \rho u\\ E\end{pmatrix}_t+\begin{pmatrix}\rho u\\ \rho u^2+p\\ \rho uH\end{pmatrix}_x=0, \tag{1}$$

where for ideal gases,

$$p=(\gamma-1)(E-\tfrac{1}{2}\rho u^2) \tag{2}$$

and γ is constant. For later reference, we denote by $\mathbf{W}=(\rho, \rho u, E)^{\mathrm{T}}$ the vector of dependent flow variables and by $\mathbf{F}(\mathbf{W})=(\rho u, \rho u^2+p, \rho uH)^{\mathrm{T}}$ the vector of flux functions.

The above set of conservation laws may also be written in nonconservation form. In particular, if we use ρ, u, and p as dependent variables, the Euler equations in primitive form are

$$\begin{pmatrix}\rho\\ u\\ p\end{pmatrix}_t+\begin{pmatrix}u & \rho & 0\\ 0 & u & \rho^{-1}\\ 0 & \gamma p & u\end{pmatrix}\begin{pmatrix}\rho\\ u\\ p\end{pmatrix}_x=0. \tag{3}$$

The two systems (1) and (3) are equivalent in smooth parts of the flow, but they are generally not equivalent if shock waves are formed. Indeed, beyond the time of shock formation, solutions to (1) are extended as *weak solutions*, using the conservation properties of the system, while weak solutions to (3) need to be defined first. Recently, a number of papers have appeared concerning the theory of weak solutions for genuinely nonconservative hyperbolic systems. This theory is of special interest in applications where the governing equations are genuinely nonconservative and for which the existing theory has to be extended (see [9] and references cited therein). The present paper deals with a different aspect of solutions to nonconservative hyperbolic systems. The equations of interest are the gas dynamics equations. They derive from conservative principles and thus possess weak solutions that are well defined and well understood. For modelling purposes which are explained later, we prefer to convert the system into a nonconservative form. The weak solutions we seek are still the ones dictated by the conservation principle. Thus, the question we ask is not what the correct weak solution of (3) is, but rather can we use (3) and still obtain the weak solutions of (1).

We now discuss extensions of the single component Euler model to the two-component case, where the two components are assumed to be two ideal gases with different γ values. In the reactive case, where the gases differ in their heat release constants, the extensions follow in complete analogy [2]. A common approach in the computation of two (or more) component flows [1, 11, 12, 20] is to define the concentration of one of the species, say species one, to be Y, describing the fraction of the mass due to species one. The concentration of species two is, accordingly, $1-Y$. If the species do not mix, then initially Y is a piecewise constant function which is either 0 or 1 everywhere, where $Y=1$ ($Y=0$) implies that the "mixture" is composed of species one (two) only. Since the model assumes no chemical reaction or diffusion, Y remains constant along streamlines,

being passively convected by the fluid and satisfies the species equation

$$Y_t + uY_x = 0. \tag{4}$$

Equation (4) may be combined with the continuity equation $(1)_a$ to form a species conseration equation,

$$(\rho Y)_t + (\rho u Y)_x = 0.$$

The pressure of the mixture is still computed from (2) but γ now depends on the composition of the mixture

$$\gamma = \frac{YC_{v_1}\gamma_1 + (1-Y)\,C_{v_2}\gamma_2}{YC_{v_1} + (1-Y)\,C_{v_2}}. \tag{5}$$

In the non-mixing case, since analytically Y is either 0 or 1, γ is either γ_1 or γ_2. Computationally, numerical diffusion induced by the numerical scheme will cause smearing in Y. Intermediate values of $0 < Y < 1$ then represent a mixture of the gas components, which is also reflected in the computation of γ in (5).

Instead of using the mass fraction Y, one may use the quantity γ itself to identify the species. Like Y, γ is a state variable which remains constant along streamlines; hence it satisfies

$$\gamma_t + u\gamma_x = 0,$$

or in conservation form,

$$(\rho\gamma)_t + (\rho u\gamma)_x = 0.$$

In this description, p is given by (2), where γ is locally computed from the quotient $\gamma = (\rho\gamma)/(\rho)$. Since γ is initially a piecewise constant function, analytically it assumes either the value γ_1 or γ_2 at all later times. Numerically, due to diffusion, "numerical mixing" occurs, reflected by intermediate values of γ. In some cases, over/undershoots in γ profiles may also occur [1, 11, 12] (see also [2] for similar phenomena in reactive flows).

In order to avoid "numerical mixing," front-tracking techniques may be used. If initially the species is separated into well-defined regions, the material interfaces can then be tracked at later times. At each point in the flow field, the fluid component is identified and the physically correct value of γ can be used. An elegant front-tracking technique, based on the notion of function level sets, has recently been proposed [13, 14] which is capable of handling complicated topological merging and breaking. In [13], this technique is applied to tracking propagating fronts in the Kelvin–Helmholtz and the Rayleigh–Taylor instabilities. One defines a distance function, ψ, that measures the distance of a given fluid particle from the material interface. Initially, $\psi = 0$ at the interface itself and is either positive or negative on either of its sides. Level sets of the function ψ propagate at the local fluid velocity; hence they satisfy the advection equation

$$\psi_t + u\psi_x = 0,$$

or in conservation form,

$$(\rho\psi)_t + (\rho u\psi)_x = 0.$$

The level set $\psi(x(t), t) = 0$ defines the propagating front at all later times. The equation of state,

$$p = (\gamma(\psi) - 1)(E - \tfrac{1}{2}\rho u^2), \tag{6}$$

now changes discontinuously across the front, separating the species:

$$\gamma(\psi) = \begin{cases} \gamma_1, & \psi < 0 \\ \gamma_2, & \psi > 0. \end{cases} \tag{7}$$

We summarize below the four extended Euler models considered in this paper. The solution of a typical Riemann problem for the extended models is illustrated in Fig. 1. The following extended Euler system is referred to as Model I,

$$\begin{pmatrix} \rho \\ \rho u \\ E \\ \rho\gamma \end{pmatrix}_t + \begin{pmatrix} \rho u \\ \rho u^2 + p \\ \rho u H \\ \rho u\gamma \end{pmatrix}_x = 0, \tag{8}$$

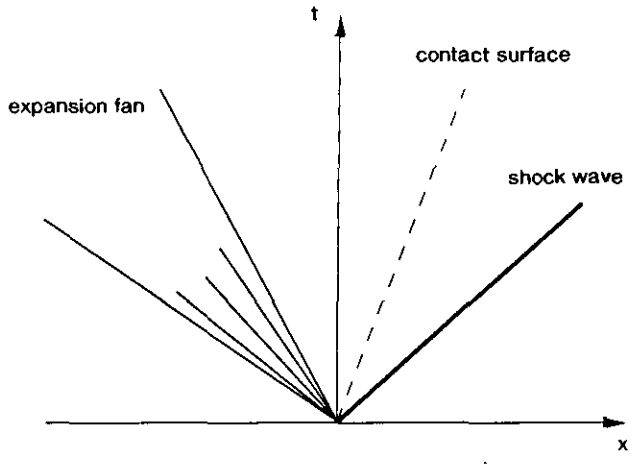

FIG. 1. Solution of a typical Riemann problem for the two species extended Euler models (8)–(11): A forward facing shock wave followed by a contact discontinuity separating the two flow components and a backward facing rarefaction wave. Note that γ changes only across the material front.

where p is calculated by (2). The following extended Euler system is referred to as Model II,

$$\begin{pmatrix} \rho \\ \rho u \\ E \\ \rho\psi \end{pmatrix}_t + \begin{pmatrix} \rho u \\ \rho u^2 + p \\ \rho u H \\ \rho u \psi \end{pmatrix}_x = 0, \tag{9}$$

where p and γ are calculated from (6) and (7). The following extended Euler system is referred to as Model III,

$$\begin{pmatrix} \rho \\ u \\ p \\ \gamma \end{pmatrix}_t + \begin{pmatrix} u & \rho & 0 & 0 \\ 0 & u & \rho^{-1} & 0 \\ 0 & \gamma p & u & 0 \\ 0 & 0 & 0 & u \end{pmatrix} \begin{pmatrix} \rho \\ u \\ p \\ \gamma \end{pmatrix}_x = 0 \tag{10}$$

with p given by (2). Finally, the following system is referred to as Model IV,

$$\begin{pmatrix} \rho \\ u \\ p \\ \psi \end{pmatrix}_t + \begin{pmatrix} u & \rho & 0 & 0 \\ 0 & u & \rho^{-1} & 0 \\ 0 & \gamma p & u & 0 \\ 0 & 0 & 0 & u \end{pmatrix} \begin{pmatrix} \rho \\ u \\ p \\ \psi \end{pmatrix}_x = 0 \tag{11}$$

with p and $\gamma(\psi)$ computed from (6) and (7).

Consistency Correction Terms for Models III and IV

The primitive formulation (3) generally yields inconsistent weak solutions due to conservation errors. In [10], we showed that shock jump conditions of primitive systems depend not only on the left and right states but also on the viscous path connecting the two. Consistent weak solutions can thus be obtained only if the equations are integrated over a consistent viscous shock profile. In [10], we also proposed a technique to modify primitive equations like (3) to have weak solutions which are consistent with weak solutions of (1) to the order of numerical approximation. The modified equations include high order viscous correction terms that account for the leading order conservation errors and are derived following an idea first introduced in [22]. One begins by assuming that (1) is solved by a given conservative scheme and that (3) is solved by a given primitive scheme. One then compares the equivalent equation that correspond to the conservative numerical scheme with that corresponding to the primitive scheme and adds/subtracts the necessary terms to make the latter identical to the former. The details of the derivation are given in [10]. Here we briefly consider one example and recall the results derived in [10]. We use the superscripts $(\,)^c$ and $(\,)^p$ to denote conservation and primitive forms, respectively. Suppose the first-order upwind scheme [18] is used to solve (1). Then the scheme is a first-order approximation to (1) but it is a second-order approximation to the *equivalent equation*,

$$\begin{aligned} \mathbf{W}_t + \mathbf{F}(\mathbf{W})_x &= \mathbf{W}_t + \mathbf{A}^c(\mathbf{W})\,\mathbf{W}_x \\ &= \frac{\Delta t}{2}\left(\frac{(|A^c|\,\mathbf{W}_x)_x}{\lambda} - \mathbf{W}_{tt}\right), \end{aligned} \tag{12}$$

where $\lambda = \Delta t/\Delta x$ denotes the mesh ratio. The terms on the right-hand side (RHS) of (12) are the leading order terms in the truncation error of the scheme. To leading order, these dissipative terms determine the viscous path across the numerical shock transition. Furthermore, this viscous path is (numerically) consistent since it is produced by a conservative scheme; hence it converges to the correct solution. Assume that (3) is also approximated by the first-order upwind scheme. Then, similarly, the scheme is a second-order approximation to the equivalent equation,

$$\tilde{\mathbf{W}}_t + A^p(\tilde{\mathbf{W}})\,\tilde{\mathbf{W}}_x = \frac{\Delta t}{2}\left(\frac{(|A^p|\,\tilde{\mathbf{W}}_x)_x}{\lambda} - \tilde{\mathbf{W}}_{tt}\right). \tag{13}$$

In general, the two viscous forms (12) and (13) are different; (13) yields physically consistent shocks while (12) does not. Let $T = \partial\tilde{\mathbf{W}}/\partial\mathbf{W}$ be the matrix transforming the conserved variables $\mathbf{W}$ to the primitive variables $\tilde{\mathbf{W}}$. Then, in order to enforce consistent viscous shock profiles on the primitive solution, the difference

$$\frac{\Delta t}{2}\mathbf{D} = \frac{\Delta t}{2}\left\{T\left(\frac{(|A^c|\,\mathbf{W}_x)_x}{\lambda} - \mathbf{W}_{tt}\right) - \left(\frac{(|A^p|\,\tilde{\mathbf{W}}_x)_x}{\lambda} - \tilde{\mathbf{W}}_{tt}\right)\right\}$$

is added to the RHS of Eq. (3). When the modified equation,

$$\tilde{\mathbf{W}}_t + A^p(\tilde{\mathbf{W}})\,\tilde{\mathbf{W}}_x = \frac{\Delta t}{2}\mathbf{D},$$

is solved by the first-order upwind scheme, it now possesses viscous shock profiles which are consistent with the order of numerical approximation. The correction terms may be simplified,

$$\mathbf{D} = \frac{T(T^{-1})_x\,|A^p|\,\tilde{\mathbf{W}}_x}{\lambda} - T(T^{-1})_t\,\tilde{\mathbf{W}}_t, \tag{14}$$

and simple algebra shows that

$$\mathbf{D} = \begin{pmatrix} 0 \\ \dfrac{1}{2\rho}\left(\dfrac{\rho_x u_x c_1 + \frac{1}{a^2}u_x p_x c_2 + \left(\frac{\rho}{a}u_x^2 + \frac{1}{\rho a}\rho_x p_x\right)c_4}{\lambda} - 4\rho_t u_t\right) \\ \dfrac{\gamma - 1}{2}\left(\dfrac{\rho u_x^2 c_3 + \frac{1}{a}u_x p_x c_4}{\lambda} - 2\rho u_t^2\right) \end{pmatrix}, \tag{15}$$

where

$$c_1 = |u-a| + 2|u| + |u+a|$$
$$c_2 = |u-a| - 2|u| + |u+a|$$
$$c_3 = |u-a| + |u+a|$$
$$c_4 = |u-a| - |u+a|.$$

By (15), **D** contains only products of first derivatives. If time derivatives are replaced by space derivatives using (3), it can be easily verified that all the products in **D** contain either u_x or p_x (or both), hence **D** vanishes near contact surfaces. We shall return to this observation when we analyze the modelling of material fronts. Models III and IV refer to the primitive formulations (10) and (11) with (15) included on the RHS. No correction is needed for the fourth component in the respective models.

3. SIMPLE WAVE ANALYSIS

Models I and II

Because of the similarity between Models I and II, the Jacobian matrices and the corresponding eigenvectors also have very similar forms. We adopt the notation in [13] and use the common letter ϕ to denote γ in the case of Model I and ψ in the case of Model II. We also use X to denote the specific internal energy i in Model I and $i\gamma'(\psi)$ in Model II.

In this common notation, the Jacobain matrix for Models I and II is [6, 7, 9]

$$A = \begin{pmatrix} 0 & 1 & 0 & 0 \\ \frac{\gamma-3}{2}u^2 - \phi X & (3-\gamma)u & (\gamma-1) & X \\ \frac{\gamma-1}{2}u^3 - uH - u\phi X & H-(\gamma-1)u^2 & \gamma u & uX \\ -\phi & \phi & 0 & u \end{pmatrix}.$$

The eigenvectors and eigenvalues of A are

$$\mathbf{r}_1 = \begin{pmatrix} 1 \\ u-a \\ H-ua \\ \phi \end{pmatrix}, \quad \mathbf{r}_2 = \begin{pmatrix} 1 \\ u \\ \frac{1}{2}u^2 \\ \phi \end{pmatrix},$$
$$\mathbf{r}_3 = \begin{pmatrix} 0 \\ 0 \\ \frac{-X}{\gamma-1} \\ 1 \end{pmatrix}, \quad \mathbf{r}_4 = \begin{pmatrix} 1 \\ u+a \\ H+ua \\ \phi \end{pmatrix} \tag{16}$$

$$\lambda_1 = u-a$$
$$\lambda_2 = u$$
$$\lambda_3 = u \tag{17}$$
$$\lambda_4 = u+a.$$

In the above, the first and fourth wave systems are acoustic waves, the second and third wave systems are entropy waves. The system has a degeneracy in that the velocity u is a double eigenvalue, and consequently the associate eigenspace is spanned by two independent eigenvectors $\mathbf{r}_2$ and $\mathbf{r}_3$. Obviously, any combination of $\mathbf{r}_2$ and $\mathbf{r}_3$ is also an eigenvector in that subspace. The above choice of $\mathbf{r}_2$ and $\mathbf{r}_3$ separates between entropy changes due to a change in γ and entropy changes due to a change in temperature (density). The only wave system that carries changes in γ itself is thus $\mathbf{r}_3$.

Small changes in the solution are determined by the eigenstructure of the matrix. So, for example, all four dependent flow variable, $\mathbf{W} = (\rho, \rho u, E, \rho\phi)^T$ change across an acoustic wave eventhough ϕ itself remains constant (this is not necessarily true if a more complex equation of state is used, see [3]). Similarly, across a contact surface, all four dependent flow variable change, even though u and p remain constant.

If a local flow fluctuation $\Delta\mathbf{W} = \mathbf{W}_R - \mathbf{W}_L$ is projected onto the characteristic fields $\mathbf{r}_k$,

$$\Delta\mathbf{W} = \sum_k \alpha_k \mathbf{r}_k,$$

then the local wave strengths α_k are given by

$$\alpha_1 = \frac{\Delta p - \rho a\,\Delta u}{2a^2}$$
$$\alpha_2 = \frac{a^2\,\Delta\rho - \Delta p}{a^2}$$
$$\alpha_3 = \rho\,\Delta\phi \tag{18}$$
$$\alpha_4 = \frac{\Delta p + \rho a\,\Delta u}{2a^2}.$$

Models III and IV

Here again we introduce a common notation ϕ to denote γ in model III and ψ in Model IV. In this notation the eigenvectors of systems III and IV are

$$\mathbf{r}_1 = \begin{pmatrix} \rho \\ -a \\ \rho a^2 \\ 0 \end{pmatrix}, \quad \mathbf{r}_2 = \begin{pmatrix} \rho \\ 0 \\ 0 \\ 0 \end{pmatrix},$$
$$\mathbf{r}_3 = \begin{pmatrix} 0 \\ 0 \\ 0 \\ 1 \end{pmatrix}, \quad \mathbf{r}_4 = \begin{pmatrix} \rho \\ a \\ \rho a^2 \\ 0 \end{pmatrix} \tag{19}$$

with eigenvalues as given in (17). In the above, the first and fourth wave systems are acoustic waves while the second and third are entropy waves. The choice of $\mathbf{r}_2$ and $\mathbf{r}_3$ clearly separates between entropy changes caused by temperature changes and those caused by changes in γ. Moreover, the above eigenstructure does reflect the fact that ϕ does not change across an acoustic front and that u and p remain constant across an entropy wave (respective entries in eigenvectors are zero). This observation is crucial for the proposed numerical algorithm and is explained in the sections that follow. Wave strengths α_k for small changes in the solution are

$$\begin{aligned}
\alpha_1 &= \frac{\Delta p - \rho a\, \Delta u}{2\rho a^2} \\
\alpha_2 &= \frac{a^2\, \Delta\rho - \Delta p}{\rho a^2} \\
\alpha_3 &= \Delta\phi \\
\alpha_4 &= \frac{\Delta p + \rho a\, \Delta u}{2\rho a^2}.
\end{aligned} \tag{20}$$

4. RIEMANN SOLVER

The first two flow models are solved by an approximate Riemann solver of Roe type [15, 16, 18], based on local linearization of the governing equations about an average state. The single gas component Roe's scheme has been extended to the multicomponent gas models by various authors [1, 2, 11–13, 17, 20]. We describe the method briefly and recall the results of its multicomponent extensions. At each cell interface, the method seeks a local linearization of the Jacobian matrix $A(\mathbf{W}) = \hat{A}(\mathbf{W}_L, \mathbf{W}_R)$, where $\mathbf{W}_L$ and $\mathbf{W}_R$ are the left and right states in the local Riemann data, so that the following condition is satisfied,

$$\hat{A}(\mathbf{W}_L, \mathbf{W}_R)\, \Delta\mathbf{W} = \Delta\mathbf{F}.$$

The single component Roe averages were obtained by requiring that the local linearization satisfies [18],

$$\begin{aligned}
\Delta\mathbf{W} &= \sum_k \alpha_k \mathbf{r}_k \\
\Delta\mathbf{F} &= \sum_k \alpha_k \lambda_k \mathbf{r}_k,
\end{aligned} \tag{21}$$

with α_k, λ_k, and $\mathbf{r}_k$ given by (16)–(18). This uniquely defines the average state

$$\begin{aligned}
\rho^* &= \sqrt{\rho_L \rho_R} \\
u^* &= \frac{\sqrt{\rho_L}\, u_L + \sqrt{\rho_R}\, u_R}{\sqrt{\rho_L} + \sqrt{\rho_R}} \\
H^* &= \frac{\sqrt{\rho_L}\, H_L + \sqrt{\rho_R}\, H_R}{\sqrt{\rho_L} + \sqrt{\rho_R}} \\
a^{*2} &= (\gamma - 1)\left(H^* - \frac{1}{2}u^2\right).
\end{aligned}$$

Roe's Linearization for Model I

The average state is derived following a similar procedure to the one in [1, 11]. The results are reported in [17] (see also [2] for a similar derivation for reactive flows) and are summarized below. In this model $X = i$. One seeks a local linearization

$$\hat{\mathbf{r}}_1 = \begin{pmatrix} 1 \\ u^* - a^* \\ H^* - u^* a^* \\ \phi^* \end{pmatrix}, \qquad \hat{\mathbf{r}}_2 = \begin{pmatrix} 1 \\ u^* \\ \frac{1}{2}u^{*2} \\ \phi^* \end{pmatrix},$$

$$\hat{\mathbf{r}}_3 = \begin{pmatrix} 0 \\ 0 \\ -\dfrac{i^*}{\gamma^* - 1} \\ 1 \end{pmatrix}, \qquad \hat{\mathbf{r}}_4 = \begin{pmatrix} 1 \\ u^* + a^* \\ H^* + u^* a^* \\ \phi^* \end{pmatrix}$$

$$\begin{aligned}
\hat{\lambda}_1 &= u^* - a^*, & \hat{\alpha}_1 &= \frac{\Delta p - \rho^* a^*\, \Delta u}{2a^{*2}} \\
\hat{\lambda}_2 &= u^*, & \hat{\alpha}_2 &= \frac{a^{*2}\, \Delta\rho - \Delta p}{a^{*2}} \\
\hat{\lambda}_3 &= u^*, & \hat{\alpha}_3 &= \rho^*\, \Delta\phi \\
\hat{\lambda}_4 &= u^* + a^*, & \hat{\alpha}_4 &= \frac{\Delta p + \rho^* a^*\, \Delta u}{2a^{*2}}
\end{aligned}$$

that satisfy (21). Solving for the average state we obtain

$$\begin{aligned}
\rho^* &= \sqrt{\rho_L \rho_R} \\
u^* &= \frac{\sqrt{\rho_L}\, u_L + \sqrt{\rho_R}\, u_R}{\sqrt{\rho_L} + \sqrt{\rho_R}} \\
H^* &= \frac{\sqrt{\rho_L}\, H_L + \sqrt{\rho_R}\, H_R}{\sqrt{\rho_L} + \sqrt{\rho_R}} \\
i^* &= \frac{\sqrt{\rho_L}\, i_L + \sqrt{\rho_R}\, i_R}{\sqrt{\rho_L} + \sqrt{\rho_R}} \\
\gamma^* &= \frac{\sqrt{\rho_L}\, \gamma_L + \sqrt{\rho_R}\, \gamma_R}{\sqrt{\rho_L} + \sqrt{\rho_R}} \\
a^{*2} &= (\gamma^* - 1)\left(H^* - \frac{1}{2}u^2\right).
\end{aligned} \tag{22}$$

Observe that since u, H, and i are linearized independently, then in general $i^* \neq a^{*2}/\gamma^*(\gamma^* - 1)$, implying that the

linearization is about a physically inconsistent average state. For conservation, the linearized sound speed must be worked out from H^* in order to satisfy (17).

Roe's Linearization for Model II

For this model, $X = i\gamma'(\psi)$ and $\gamma(\psi)$ is a step function. The derivative $\gamma'(\psi)$ thus involves the $\delta(\psi - 0)$ function which must be approximated numerically in the process of obtaining local flow averages. The full details of this derivation are given in [13]. Here we briefly summarize the results. The required average state is

$$\rho^* = \sqrt{\rho_L \rho_R}$$

$$u^* = \frac{\sqrt{\rho_L}\, u_L + \sqrt{\rho_R}\, u_R}{\sqrt{\rho_L} + \sqrt{\rho_R}}$$

$$H^* = \frac{\sqrt{\rho_L}\, H_L + \sqrt{\rho_R}\, H_R}{\sqrt{\rho_L} + \sqrt{\rho_R}}$$

$$\psi^* = \frac{\sqrt{\rho_L}\, \psi_L + \sqrt{\rho_R}\, \psi_R}{\sqrt{\rho_L} + \sqrt{\rho_R}}$$

$$a^{*2} = (\gamma - 1)\left(H^* - \frac{1}{2} u^{*2}\right).$$

An additional condition is that X^* satisfies

$$X^* \rho^* \, \Delta\psi = \Delta p - (\gamma^* - 1)\, \Delta \frac{p}{\gamma - 1}$$

which is used to determine X^* in terms of γ^*,

$$X^* = \frac{\Delta p - (\gamma^* - 1)\, \Delta p/(\gamma - 1)}{\rho^* \, \Delta\psi}. \tag{23}$$

Equation (23) places a differential condition on γ^* which cannot be satisfied (for details see [13]); hence an arbitrary choice is made for γ^*,

$$\gamma(\psi) = \frac{(\psi - \psi_L)\, \gamma_R + (\psi - \psi_R)\, \gamma_L}{\psi_R - \psi_L}. \tag{24}$$

Then we use $\gamma^* = \gamma(\psi^*)$, where ψ^* is given above. Here again, conditions (21) are not satisfied consistently.

Local Linearization of Models III and IV

Models III and IV are also solved by a Roe-type solver based on a local linearization of the governing equations about an average state. Since the models are not conservative, the linearized equations are not used to construct a Godunov-type Riemann solver [5]. Instead, the fluctuation and signal framework [16] is used to integrate the equations. Because of the fundamental lack of conservation, there does not seem to be a theoretical justification to use the elaborate averages (22). In the calculation below, simple arithmetic averages are used,

$$\rho^* = \frac{\rho_L + \rho_R}{2}$$

$$u^* = \frac{u_L + u_R}{2}$$

$$p^* = \frac{p_L + p_R}{2}$$

$$\gamma^* = \frac{\gamma_L + \gamma_R}{2}$$

$$\left(\psi^* = \frac{\psi_L + \psi_R}{2}\right).$$

The correction terms use point values of flow variables and centered differencing for the derivatives. We note that in [21], the elaborate averages (22) were reported to be superior.

5. NUMERICAL INTERFACE MODELLING

The oscillations near the material front may be explained by a fundamental incompatibility between the conservative simple wave models (i.e., eigenvectors) of (8) and (9) and material interface data. Indeed, any smearing that occurs in the conserved variables, due to numerical diffusion, immediately generates pressure fluctuations across the material front. These oscillations are totally erroneous; once generated they subsequently contaminate the flow field. Consider Riemann data that correspond to a propagating material front, with $p_L = p_R$ and $u_L = u_R$. In what follows we show that as soon as the pressure is computed from numerically smeared profiles of the conserved quantities, its computed value, which should remain $p = p_L = p_R$, has an error δp proportional to the jump in the data, Δ, raised to some power s (see Fig. 2). The erroneous pressure waves $\delta p = O(\Delta)^s$ then infiltrate the density and velocity fields. We now show that for Model I, $s = 2$, and for Model II, $s = 1$, which explains why oscillations are much more visible in the latter case. We also show that for Models III and IV, $\delta p = 0$; that is, material fronts are computed exactly, even though the governing equations are not in conservation form (see also [8] for related discussion). Finally, we show that in the single component conservative model, $\delta p = 0$; that is the problem of erroneous pressure fluctuations due to numerical diffusion does not exist in the single-component Euler model (1).

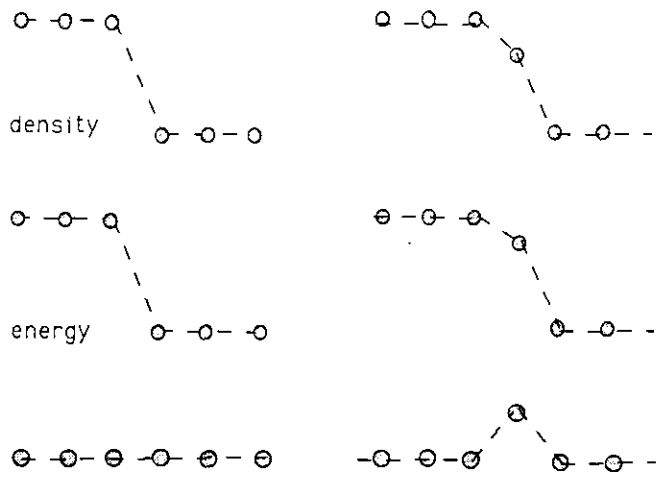

FIG. 2. A pressure fluctuation $\delta p = O(\Delta)^s$ causes erroneous pressure waves near material interface, when pressure is computed from smeared profiles of conserved flow variables. The fluctuation subsequently infiltrates other flow variables and contaminates solution.

Model I

Consider the computational interval $(j-1, j)$ and assume that the initial data correspond to a simple material interface (no density gradient),

$$\begin{aligned} &\rho_L = \rho_R = \rho \\ &p_L = p_R = p \\ &u_L = u_R = u \qquad (u > 0) \\ &\gamma_L \neq \gamma_R. \end{aligned}$$

In the exact solution, ρ, u, and p remain constant and γ is (linearly) advected downstream at a constant speed u, i.e., $\gamma(x, t) = \gamma(x - ut, 0)$.

For the above data $\alpha_1 = \alpha_2 = \alpha_4 = 0$. Since we assume $u > 0$, the first-order upwind scheme gives

$$\mathbf{W}_j^{n+1} = \mathbf{W}_j^n - \frac{\Delta t}{\Delta x} \alpha_3 \lambda_3 \mathbf{r}_3$$

and by $\mathbf{r}_3$ in (16), this yields changes in E_j and $(\rho\gamma)_j$ only. The newly computed conserved variables are

$$\begin{aligned} \rho_j^{n+1} &= \rho_j^n \\ (\rho u)_j^{n+1} &= (\rho u)_j^n \\ E_j^{n+1} &= E_j^n - \frac{\Delta t}{\Delta x} u^* \rho^* \frac{-i^*}{\gamma^* - 1} \Delta\gamma \\ (\rho\gamma)_j^{n+1} &= (\rho\gamma)_j^n - \frac{\Delta t}{\Delta x} u^* \rho^* \Delta\gamma \end{aligned} \tag{25}$$

and, by $(25)_{a,b}$, $\rho_j^{n+1} = \rho_j^n = \rho$ and $u_j^{n+1} = u_j^n = u$. Also by $(25)_d$,

$$\gamma_j^{n+1} = \gamma_j^n - \frac{\Delta t}{\Delta x} u^* \Delta\gamma. \tag{26}$$

Observe that for the above data, the density square root averaging (22) gives $\rho^* = \rho$, $u^* = u$, and

$$\begin{aligned} \gamma^* &= \frac{\gamma_L + \gamma_R}{2} \\ i^* &= \frac{p}{2\rho}\left(\frac{1}{\gamma_L - 1} + \frac{1}{\gamma_R - 1}\right). \end{aligned} \tag{27}$$

The new value of p is obtained using the equation of state (2),

$$\begin{aligned} p_j^{n+1} &= (\gamma_j^{n+1} - 1)\left(E_j^{n+1} - \frac{1}{2}(\rho u^2)_j^{n+1}\right) \\ &= \left(\gamma_j^n - \frac{\Delta t}{\Delta x} u \Delta\gamma - 1\right)\left(E_j^n + \frac{\Delta t}{\Delta x} u\rho \frac{i^*}{\gamma^* - 1} \Delta\gamma - \frac{1}{2}\rho u^2\right) \\ &= \left(\gamma_R - 1 - \frac{\Delta t}{\Delta x} u \Delta\gamma\right)\left(E_j^n - \frac{1}{2}\rho u^2 + \frac{\Delta t}{\Delta x} u\rho \frac{i^*}{\gamma^* - 1} \Delta\gamma\right) \\ &= (\gamma_R - 1)\left(E_j^n - \frac{1}{2}(\rho u^2)\right) - \frac{\Delta t}{\Delta x} u \left(E_j^n - \frac{1}{2}\rho u^2\right) \Delta\gamma \\ &\quad + \frac{\Delta t}{\Delta x} u\rho (\gamma_R - 1) \frac{i^*}{\gamma^* - 1} \Delta\gamma \\ &\quad - \left(\frac{\Delta t}{\Delta x} u\right)^2 \rho \frac{i^*}{\gamma^* - 1} (\Delta\gamma)^2 \\ &= p + \delta p. \end{aligned}$$

After rearrangement, using (26) and (27), the error terms of order $\Delta\gamma$ cancel out and we obtain

$$\delta p = u^* \frac{\Delta t}{\Delta x}\left(1 - u^* \frac{\Delta t}{\Delta x}\right) \frac{p}{(\gamma_L - 1)(\gamma_R - 1)} (\Delta\gamma)^2.$$

For a stable scheme, $u^*(\Delta t/\Delta x) < 1$, and thus $\delta p = O(\Delta\gamma)^2$ is always positive. This erroneous pressure fluctuation cancels out at later time steps, as soon as a velocity divergence arises to balance it. This velocity divergence can clearly be seen in Figs. 3 and 4, and also in the figures in Refs. [1, 11, 12]. The velocity increases in the downstream direction and decreases in the upstream direction.

Model II

For the same initial data, expressed in terms of the distance function ψ,

$$\rho_L = \rho_R = \rho$$
$$p_L = p_R = p$$
$$u_L = u_R = u \qquad (u > 0)$$
$$\psi_L \neq \psi_R,$$

the only nonzero wave strength in (18) is α_3, which again yields changes in E_j and $(\rho\psi)_j$ only. In analogy with Model I, we obtain $\rho_j^{n+1} = \rho_j^n = \rho$ and $u_j^{n+1} = u_j^n = u$. We also obtain

$$E_j^{n+1} = E_j^n + \frac{\Delta t}{\Delta x} u^* \rho^* \frac{X^*}{\gamma^* - 1} \Delta\psi$$
$$\psi_j^{n+1} = \psi_j^n - \frac{\Delta t}{\Delta x} u^* \Delta\psi,$$

where we recall that $\rho^* = \rho$, $u^* = u$, and that by (19) and (20),

$$X^* = \frac{\Delta p - (\gamma^* - 1)\,\Delta(p/(\gamma - 1))}{\rho^* \Delta\psi}$$
$$\gamma^* = \gamma(\psi^*) = \frac{(\psi^* - \psi_L)\gamma_R + (\psi^* - \psi_R)\gamma_L}{\psi_R - \psi_L}$$
$$\psi^* = \frac{\sqrt{\rho_L}\psi_L + \sqrt{\rho_R}\psi_R}{\sqrt{\rho_L} + \sqrt{\rho_R}} = \frac{1}{2}(\psi_L + \psi_R).$$

The newly computed E becomes

$$E_j^{n+1} = E_j^n - \frac{\Delta t}{\Delta x} u\,\Delta\left(\frac{p}{\gamma - 1}\right)$$
$$= E_j^n - \frac{\Delta t}{\Delta x} up\left(\frac{1}{\gamma_R - 1} - \frac{1}{\gamma_L - 1}\right)$$

and the new pressure is

$$p_j^{n+1} = (\gamma(\psi_j^{n+1}) - 1)\left\{E_j^{n+1} - \frac{1}{2}(\rho u)_j^{2n+1}\right\}$$
$$= (\gamma(\psi_j^{n+1}) - 1)$$
$$\times \left\{E_j^n - \frac{\Delta t}{\Delta x} up\left(\frac{1}{\gamma_R - 1} - \frac{1}{\gamma_L - 1}\right\} - \frac{1}{2}\rho u^2\right)$$
$$= (\gamma(\psi_j^{n+1}) - 1)$$
$$\times \left\{\frac{p}{\gamma_R - 1} - \frac{\Delta t}{\Delta x} up\left(\frac{1}{\gamma_R - 1} - \frac{1}{\gamma_L - 1}\right)\right\}.$$

Here we need to distinguish between two possible cases. If $u(\Delta t/\Delta x)$ is such that $\psi_j^{n+1} > 0$, then $\gamma(\psi_j^{n+1}) = \gamma_R$ and

$$p_j^{n+1} = (\gamma_R - 1)\left\{\frac{p}{\gamma_R - 1} - \frac{\Delta t}{\Delta x} up\left(\frac{1}{\gamma_R - 1} - \frac{1}{\gamma_L - 1}\right)\right\}$$
$$= p - \frac{\Delta t}{\Delta x} up\left(1 - \frac{\gamma_R - 1}{\gamma_L - 1}\right)$$
$$= p + \frac{\Delta t}{\Delta x} u\left(\frac{p}{\gamma_L - 1}\right)[\gamma].$$

If $u(\Delta t/\Delta x)$ is such that $\psi_j^{n+1} < 0$, then $\gamma(\psi_j^{n+1}) = \gamma_R$ and

$$p_j^{n+1} = (\gamma_L - 1)\left\{\frac{p}{\gamma_R - 1} - \frac{\Delta t}{\Delta x} up\left(\frac{1}{\gamma_R - 1} - \frac{1}{\gamma_L - 1}\right)\right\}$$
$$= \left(\frac{\gamma_L - 1}{\gamma_R - 1}\right)p - \frac{\Delta t}{\Delta x} up\left(\frac{\gamma_L - 1}{\gamma_R - 1} - 1\right)$$
$$= p - \frac{p}{\gamma_R - 1}\left(1 - \frac{\Delta t}{\Delta x} u\right)[\gamma].$$

In either situation, $\delta_p = O[\gamma]$, where $[\gamma] = \gamma_R - \gamma_L$ is the jump in the γ values of the two gas components. Note that this is different from $\Delta\gamma$ which denotes the partial jump in γ in the diffused γ profile. Also note that $\Delta\gamma$ which denotes the partial jump in γ in the diffused γ profile. Also note that $\Delta\gamma$ is generally smaller in magnitude. Model II thus generates erroneous pressure waves δp which are an order of magnitude larger than Model I. Note also that δp does not have a definite sign (it has opposite signs in the respective cases); hence it creates both over/undershoots in the pressure field and, consequently, in the rest of the flow variables.

Models III and IV

For the same Riemann problem, the only nonzero wave strength is again α_3, except that this time the only flow quantity that changes is ϕ, while δp, δp, and δu are identically zero, as in the exact solution. The newly computed ϕ value, which is either γ or ψ, is

$$\phi_j^{n+1} = \phi_j^n - \frac{\Delta t}{\Delta x} u^* \Delta\phi.$$

Since the propagation speed $u^* = u$ is exact, the numerical scheme is in fact *exact*. Equations (10), (11), although nonconservative, reduce to *linear* advection of ϕ; thus they become exact near the material interface and no conservation errors are committed. The same is true for data corresponding to an entropy wave caused by a temperature gradient ($\delta\mathbf{W} \propto \mathbf{r}_2$). In this case, the governing equations reduce to linear advection of ρ at the physically correct speed u. We also note that the viscous perturbations (15) do not play any role near contact surfaces, since all the terms

in (15) contain either velocity gradients or pressure gradients (or both); hence they vanish. This is expected since the inviscid model is exact.

The Single Component Euler Model

To analyze the single component case, we use Model I, but we ignore its fourth component which becomes redundant if $\gamma_L = \gamma_R$. The contact surface we consider corresponds to a temperature discontinuity, with data $p_L = p_R$, $u_L = u_R$, but $\rho_L \neq \rho_R$. The only nonzero wave strength is $\alpha_2 = \Delta\rho$, yielding changes in all three flow variables,

$$\begin{pmatrix} \rho_j^{n+1} \\ (\rho u)_j^{n+1} \\ E_j^{n+1} \end{pmatrix} = \begin{pmatrix} \rho_j^n \\ (\rho u)_j^n \\ E_j^n \end{pmatrix} + u\frac{\Delta t}{\Delta x}\begin{pmatrix} 1 \\ u \\ \frac{1}{2}u^2 \end{pmatrix},$$

$$\Delta\rho = \begin{pmatrix} \rho_j^n + \delta\rho \\ (\rho u)_j^n + \delta(\rho u) \\ E_j^n + \delta E \end{pmatrix}. \tag{28}$$

The newly computed pressure is

$$p_j^{n+1} = (\gamma - 1)\left(E_j^{n+1} - \frac{1}{2}\frac{[(\rho u)_j^{n+1}]^2}{\rho_j^{n+1}}\right). \tag{29}$$

Using $\rho + \delta\rho$ to denote the new density and, similarly, $p_j^{n+1} = p + \delta p$, $(\rho u)_j^{n+1} = \rho u + \delta(\rho u)$, and $E_j^{n+1} = E + \delta E$, we obtain

$$\begin{aligned}(p + \delta p)(\rho + \delta\rho) &= (\gamma - 1) \\ &\quad \times [(E + \delta E)(\rho + \delta\rho) - \tfrac{1}{2}(\rho u + \delta(\rho u))^2] \\ &= (\gamma - 1)[(E - \tfrac{1}{2}\rho u^2)\rho + (E - \tfrac{1}{2}\rho u^2)\,\delta\rho] \\ &= (\gamma - 1)[(E - \tfrac{1}{2}\rho u^2)(\rho + \delta\rho)] \\ &= p(\rho + \delta\rho), \end{aligned} \tag{30}$$

where we have used (28) to express all the fluctuations in terms of density fluctuations $\delta\rho$, namely, $\delta(\rho u) = (u)\,\delta\rho$ and $\delta E = (\frac{1}{2}u^2)\,\delta\rho$.

We thus obtain that $\delta p = 0$ and the problem of erroneous pressure fluctuations does not exist in the single component gas model. It arises only when the contact surface separates materials of different chemical types.

6. NUMERICAL TESTS

We consider the Sod's shock-tube problem [19], with two different ideal gases. The initial data give the Riemann problem

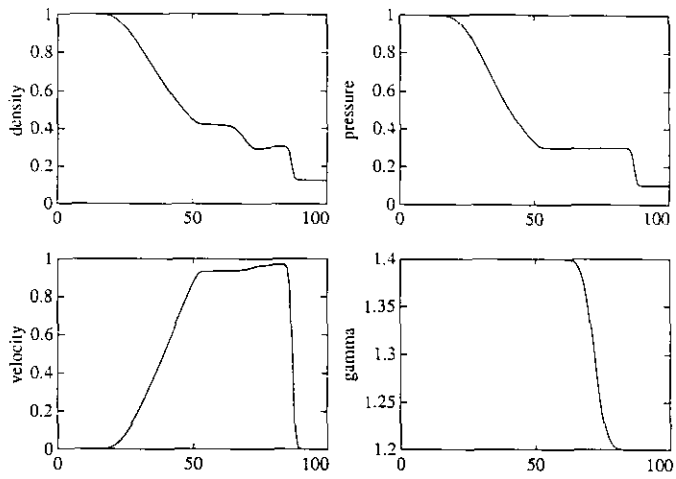

FIG. 3. Computation with Model I by a first-order upwind scheme.

$$\begin{aligned} \rho_L &= 1.0, & \rho_R &= 0.125 \\ u_L &= 0.0, & u_R &= 0.0 \\ p_L &= 1.0, & p_R &= 0.1 \\ \gamma_L &= 1.4, & \gamma_R &= 1.2. \end{aligned}$$

The same problem has been considered by Larrouturou and Fezoui [12] and by Abgrall in [1]. The results shown are obtained by the extended Roe's approximate Riemann solver for first- and second-order upwind schemes. Figures 3–4 show results obtained by Model I. A dip in the density profile is clearly visible just ahead of the material interface. We also observe a nonphysical step in the velocity across the contact surface, the velocity being higher ahead of the contact and lower behind it. This is in "agreement" with the analysis showing that the erroneous pressure fluctuations δp are always positive. This generates acoustic waves which travel in both up/downstream directions, yielding a velocity increase downstream and a velocity

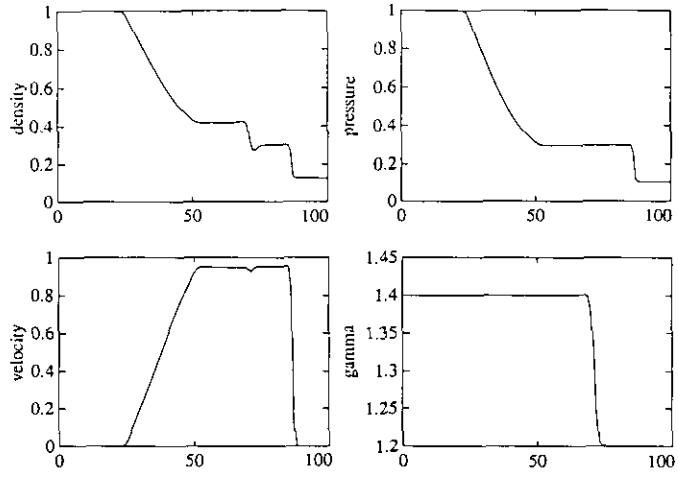

FIG. 4. Computation with Model I by a second-order upwind scheme.

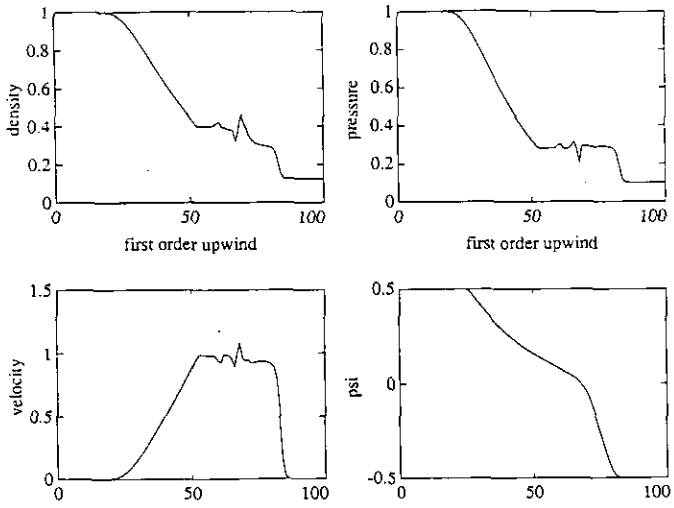

FIG. 5. Computation with Model II by a first-order upwind scheme.

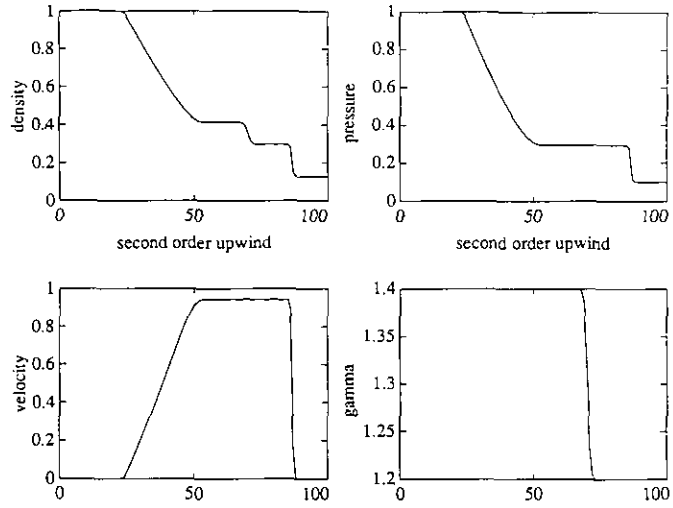

FIG. 7. Computation with Model III by a second-order upwind scheme.

decrease upstream (Fig. 3). The pressure field itself maintains a reasonably uniform profile across the contact surface. Computations with a second-order upwind scheme tend to improve results but a "hicc up" in the solution is still visible near the contact. Similar observations were also made in Refs. [1, 11, 12].

Figures 5–6 show results obtained by Model II. Both first- and second-order calculations are contaminated by strong oscillations in all flow variables. The randomness in fluctuation patterns agrees with δp not having a definite sign. The only variable that is not contaminated by oscillations is the distance function ψ, possibly due to "in phase" oscillations of the variables ρ and $\rho\phi$. Going to higher order schemes tend to reduce the amplitude of the oscillations, but they are still very visible (Fig. 6).

Figure 7 is obtained by Model III. The oscillations in all flow variables are completely eliminated, as predicted by the simple wave analysis. Conservation errors, although not totally removed, are of an acceptably low level. The reader is referred to Ref. [10] for an extensive numerical study of the level of conservation errors and the range of validity of the proposed scheme. Results obtained by Model IV (Fig. 8) are very similar to the ones obtained by Model III. This indicates that, at least for this problem, allowing γ to diffuse (Model III) has only a negligible effect on the computed solution, over using the piecewise constant γ values (Model IV).

Convergence Tests

The spurious velocity divergence in Fig. 3 is alarming and calls for numerical convergence tests to determine if the error decreases and how fast. To study this, we conducted a

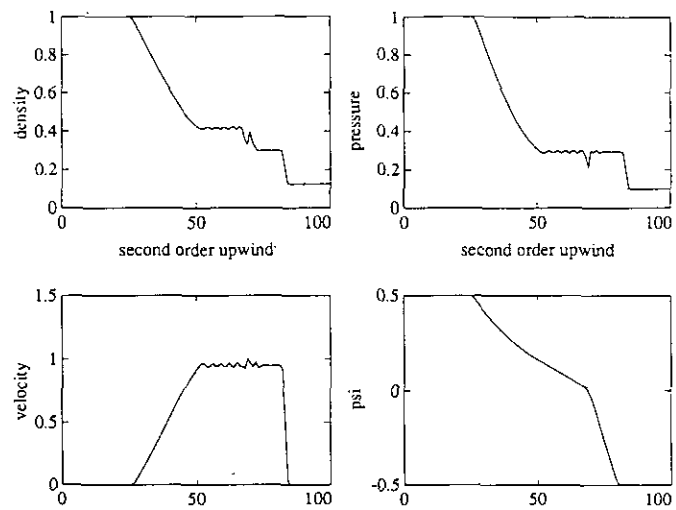

FIG. 6. Computation with Model II by a second-order upwind scheme.

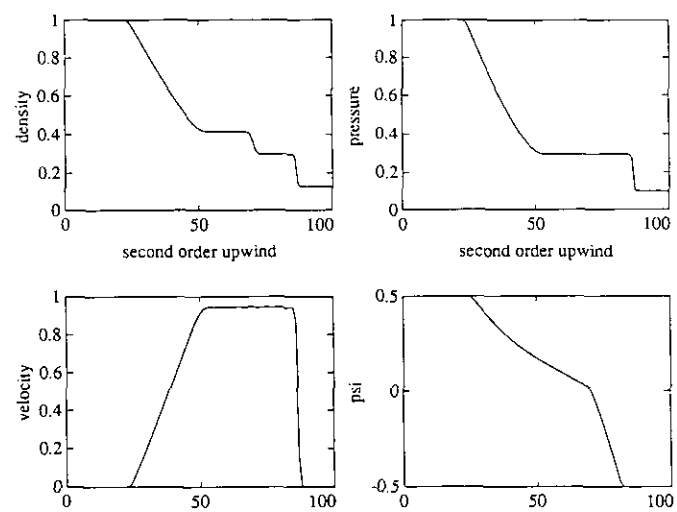

FIG. 8. Computation with Model IV by a second-order upwind scheme.

sequence of computations on increasingly fine meshes. For convenience of comparison, the results are superimposed and a close-up of the solution profiles near the material interface is shown in Figs. 9 (first-order upwind scheme) and Fig. 10 (second-order upwind scheme). They suggest two things:

(a) The nonphysical velocity jump across the contact tends to decrease with mesh refinement. The rate of decrease, however, is extremely slow. Even without a close inspection, a jump in velocity is still visible on the finest 1600-point mesh calculation.

(b) The undershoot in ρ does not vanish even on the finest mesh. While the first-order calculations (Fig. 9) seem stable near the contact surface, the second-order calculations (Fig. 10) clearly show an instability as the oscillation grows with mesh refinement.

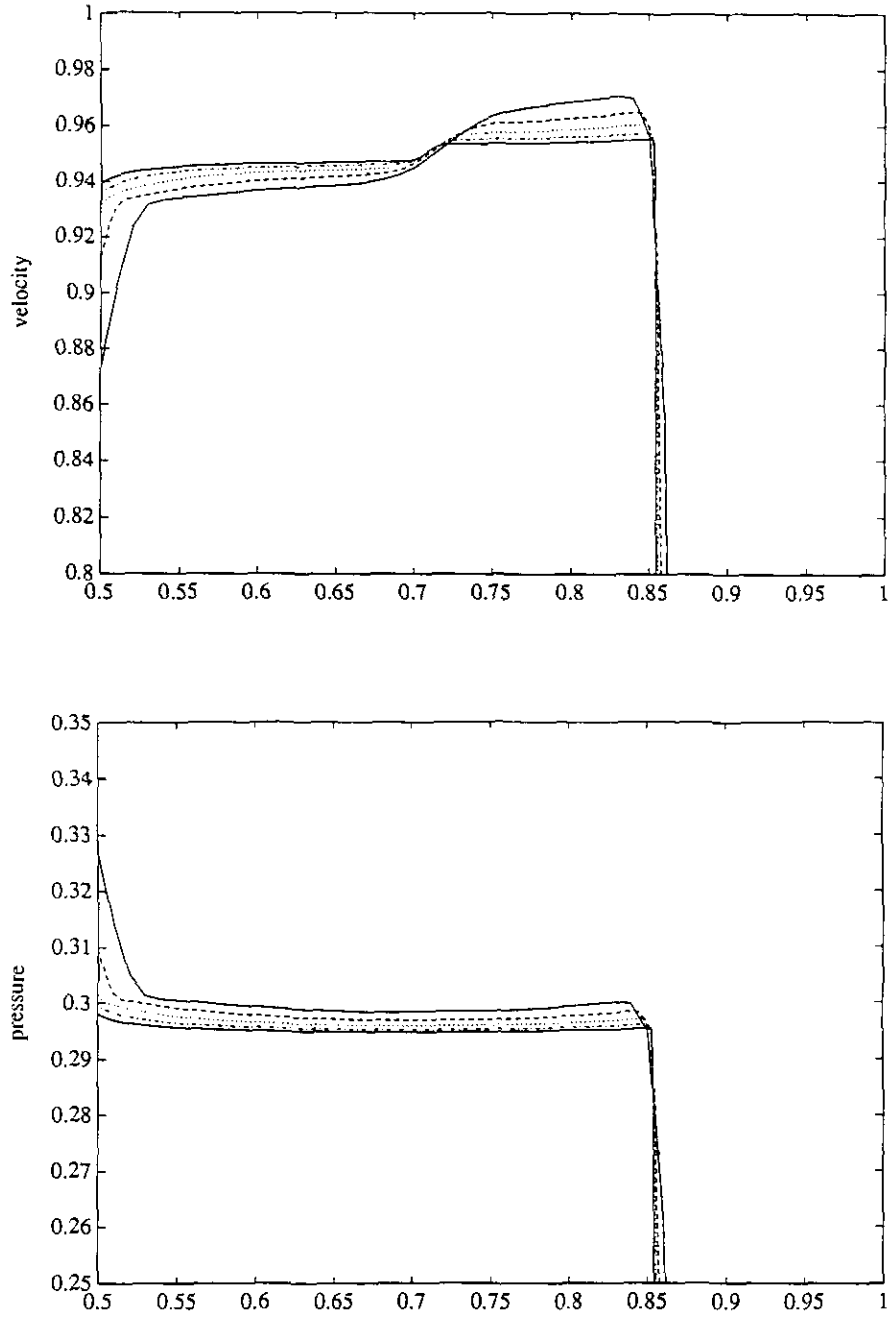

FIG. 9. Convergence test with Model I by a first-order upwind scheme: (a) velocity profile; (b) pressure profile.

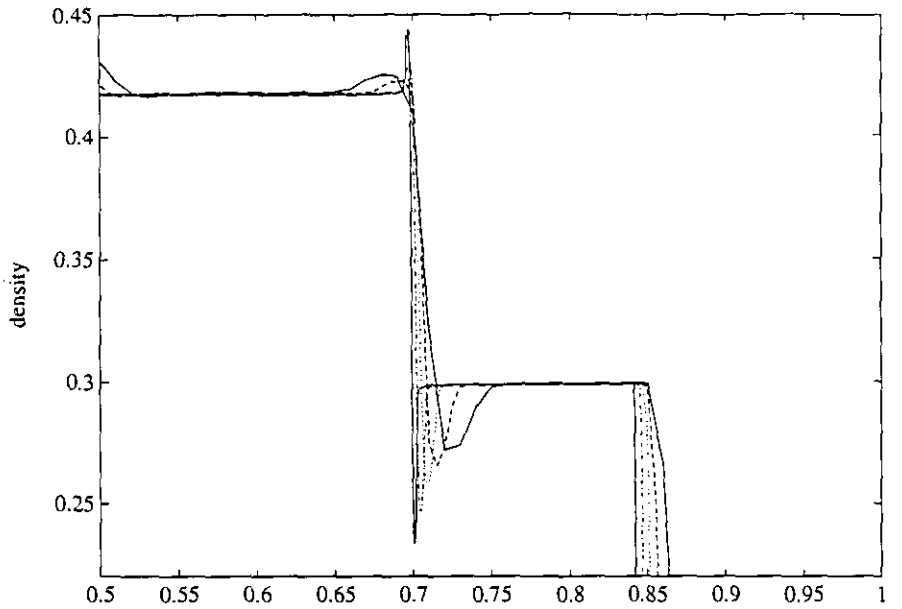

FIG. 10. Convergence test with Model I by a second-order upwind scheme: density profile.

REFERENCES

1. R. Abgrall, *Rech. Aerosp.* **6**, 31 (1988).
2. J. F. Clarke, S. Karni, J. J. Quirk, P. L. Roe, L. G. Simmonds, and E. F. Toro, Cranfield CoA Report 9013, 1990, *J. Comput. Phys.* **106**, 215 (1993).
3. P. Colella and H. M. Glaz, *J. Comput. Phys.* **59** (2), 264 (1985).
4. B. Engquist and B. Sjogreen, UCLA CAM Report 91-03.
5. S. K. Godunov, *Math. Sb.* **47**, 271 (1959).
6. E. Harabetian and R. Pego, IMA Preprint Series 743, December 1990; *J. Comput. Phys.*,
7. A. Harten, *J. Comput. Phys.* **83**, 148 (1989).
8. T. Y. Hou and P. D. Lax, *Commun. Pure Appl. Math.* **44**, 1 (1991).
9. T. Y. Hou and Ph. Le Floch, preprint, 1991.
10. S. Karni, *SIAM J. Numer. Anal.* **29** (6), 1592 (1992).
11. B. Larrouturou, *J. Comput. Phys.* **95**, 59 (1991).
12. B. Larrouturou and L. Fezoui, "On the Equations of Multi-component Perfect or Real Gas Inviscid Flow," in *Non-linear Hyperbolic Problems*, edited by Carasso, Charrier, Hanouzet, and Joly, Lecture Notes in Mathematics, Vol. 1402, (Springer-Verlag, Heidelberg, 1989), p. 69.
13. W. Mulder, S. Osher, and J. A. Sethian, *J. Comput. Phys.* **100**, 209 (1992).
14. S. Osher and J. A. Sethian, *J. Comput. Phys.* **79** (1), 12 (1988).
15. P. L. Roe, *J. Comput. Phys.* **43**, 357 (1981).
16. P. L. Roe, "Fluctuations and Signals; A Framework for Numerical Evolution Problems," in *Numerical Methods for Fluid Dynamics*, edited by K. W. Morton and M. J. Baines (Academic Press, New York/London, 1982).
17. P. L. Roe, A new approach to computing discontinuous flows of several ideal gases, 1989 (unpublished).
18. P. L. Roe and J. Pike, "Efficient Construction and Utilization of Approximate Riemann Solutions," in *Computing Methods in Applied Sciences and Engineering, VI*, edited by R. Glowinski and J.-L. Lions, (Elsevier, New York, 1984).
19. G. A. Sod, *J. Comput. Phys.* **27**, 1 (1977).
20. S. P. Spekreijse and R. Hagmeijer, "Derivation of a Roe Scheme for an N-Species Chemically Reacting Gas in Thermal Equilibrium," in *Non-linear Hyperbolic Problems*, edited by Carasso, Charrier, Hanouzet and Joly, Lecture Notes in Mathematics, Vol. 1402 (Springer-Verlag, Heidelberg, 1989), p. 522.
21. F. de Vuyst, ONERA Report, Office National d'Etudes et Recherches Aerospatiales, France, 1991 (unpublished).
22. G. Zwas and J. Roseman, *J. Comput Phys.* **12**, 179 (1973).